Available online at www.sciencedirect.com
SCIENCE DIRECT
Journal of Catalysis 234 (2005) 364–375
JOURNAL OF CATALYSIS
www.elsevier.com/locate/jcat

Role of bulk and grain boundary oxygen mobility in the catalytic oxidation activity of $LaCo_{1-x}Fe_xO_3$

S. Royer [a], D. Duprez [b], S. Kaliaguine [a,*]

[a] *Department of Chemical Engineering, Laval University, Quebec G1K 7P4, Canada*
[b] *LACCO, UMR CNRS 6503, Université de Poitiers, 40 Av. du Recteur Pineau, F-86022 Poitiers cedex, France*

Received 22 September 2004; revised 18 November 2004; accepted 22 November 2004

Available online 10 August 2005

Abstract

In this study, oxygen mobility in $LaCoO_3$ was studied by means of oxygen isotopic exchange. Seven $LaCoO_3$ were synthesized by different methods and characterized. The solids present large differences in specific surface area, crystallite size, and redox properties (as measured by oxygen desorption and reduction by H_2). The results obtained for the exchange reaction showed that the activity was strongly influenced by the crystal size. However, it was observed for all of the solids, that all of the bulk oxygen atoms are available for exchange. A mechanism of exchange is proposed that supposes the adsorption of an O_2 molecule to a reduced cobalt site. Then the adsorbed O_2 exchanges with the surface, and the exchanged atom can diffuse into the grain boundaries and into the bulk of the solid. It is supposed, from these results, that grain boundary diffusion proceeds quickly in comparison with bulk diffusion. These results were compared with those obtained for the CH_4 oxidation reaction. The mechanism of oxidation was discussed on the basis of a comparison of the results obtained for these two reactions.

Keywords: Perovskite; Oxygen isotopic exchange; Oxygen mobility; CH_4 oxidation

1. Introduction

Perovskites are mixed oxides with the general formula ABO_3. Many different compositions were found to be possible for these solids requiring that the electro-neutrality be maintained, and the A and B cations are stable in dodecahedral and octahedral environments, respectively. However, only a small number of the possible compositions were found to present an interesting activity for gas-phase oxidation reactions. Libby [1] was the first to report a high activity of some cobalt and manganese-based perovskites for catalytic oxidation reactions. In some cases, perovskites were found to be as active as conventional supported noble metal catalysts [2,3], in spite of their low specific surface areas. This explains why, during the last 30 years, an intense effort has been made to increase activity and to reach a comprehensive view of the oxidation mechanism [4]. The activity was found to be mainly dependent on the nature of the transition metal in the B position, more than on the nature of the A cation (as long as A is a lanthanide). The activity was generally found to vary as follows: $ACoO_3 \approx AMnO_3 > ANiO_3 > AFeO_3 \gg ACrO_3$ [5,6]. To increase the activity, many authors replaced part of the A and/or B with cations of other valences. An increase in activity was clearly observed in the case of La^{3+} replacement with Sr^{2+} or Ce^{4+} [7–11]. A change in the valence of the B cation (Co^{3+}/Co^{2+} or Mn^{3+}/Mn^{4+}) results from these substitutions. Moreover, some adjustment of the anionic or cationic vacancy concentration in the crystal is also supposed to maintain the electroneutrality. All of these structural changes strongly modify the reducibility of the B cation, and then the oxygen mobility in the perovskite, as observed by temperature-programmed reduction (TPR) and oxygen thermo-desorption (TPD-O_2). Misono et al. [6,7,12] were the first to use TPD-O_2 as a measure of oxygen mobility. By this method, the authors distinguished two kinds of oxygen. The first one, designated as

* Corresponding author. Fax: +1-418-656-3810.
E-mail address: kaliagui@gch.ulaval.ca (S. Kaliaguine).

0021-9517/$ – see front matter
doi:10.1016/j.jcat.2004.11.041

α-oxygen, is supposed to desorb from the surface of the solid (O^- or O_2^- species). The second one, β-oxygen, because of the large amount desorbed, is supposed to originate from the bulk of the solid (O^{2-}), with simultaneous reduction of some Co^{3+} into Co^{2+}. The interpretation of the oxidation reaction mechanisms was made on the basis of the results of oxygen desorption and the temperatures at which surface and bulk oxygens become reactive [13]. Then, for low-temperature reactions, like CO oxidation, a suprafacial mechanism with the participation of surface oxygen is proposed. For high temperature reactions, an intrafacial mechanism, involving the lattice oxygens, is preferred. Nevertheless, a recent study of the properties of some $LaCoO_3$ prepared by different methods [14] showed that the activity for the CH_4 oxidation reaction cannot be correlated with the properties of the samples in TPD-O_2. This study also revealed that the β-oxygen does not desorb from the crystal lattice but results from the reduction of some Co^{3+} segregated in the grain boundaries. The higher rates of oxygen diffusion in the grain boundaries compared with the bulk of the crystals, as observed by Sakai et al. [15,16], justify this interpretation. Moreover, the results obtained for the CH_4 oxidation reaction led us to suppose an important effect of the bulk oxygen mobility on the catalytic activity [14], even though the activities observed for this reaction do not correlate with the properties observed for TPD-O_2.

In this work, oxygen isotopic exchange (OIE) was used to measure oxygen mobility. The physical, redox, and catalytic properties of the samples studied in this work were described in two previous works [14,17]. It was observed that among the various catalysts the large differences in activities for the CH_4 oxidation reaction were not unequivocally related to the specific surface area. Moreover, it was concluded that TPD-O_2 was not an appropriate method for measuring oxygen mobility or surface or bulk reactivity. Oxygen isotopic exchange measurements, performed on some supported noble metal catalysts [18–22], permitted access to the surface reactivity (by measurement of the initial exchange reaction rate) and to the bulk oxygen mobility. However, such results for the perovskites are scarce [7,8,12,23]. Under these considerations, OIE experiments were designed to explain, in terms of oxygen mobility, the differences in specific activity observed for the methane oxidation reaction.

2. Experimental

2.1. Materials

Seven $LaCo_{1-x}Fe_xO_3$ samples, synthesized by different procedures, were used for the OIE reaction (OIE).

Five samples were first prepared by different methods: solid-state reaction (SS), coprecipitation (COP), citrate complexation (CIT), and reactive grinding of the single oxides (RG) and of an amorphous precursor (COPRG). The details of the synthesis procedures can be found in Ref. [14]. Table 1 summarizes some of the physical properties of these solids. The SS, COP, and CIT samples were prepared by conventional methods. For these solids, the calcination temperatures, necessary to obtain the total conversion of the precursors into perovskite, vary from 600 to 1000 °C. Then, large differences in crystal domain size (D_1) and specific surface area (S_{BET}) are observed (Table 1). As mentioned above, the RG sample was prepared by reactive grinding. This method involves the replacement of the thermal energy, necessary for the crystallization, with the mechanical energy exercised during grinding. Then, perovskites are crystallized near the ambient temperature, and solids with very large specific surface areas can be obtained [24,25]. RG was synthesized in two steps. The single oxides were first ground for 4 h under O_2, in a SPEX laboratory grinder (rotation speed = 1040 rpm). At the end of this step, the single oxide conversion into perovskite is complete. The second step of grinding (20 h) was done with ZnO added to the perovskite. This step results in an in crease of the specific surface area developed by the solid. The COPRG sample was synthesized under the same grinding conditions as RG, but

Table 1
Physical properties and first order rate parameters for the CH_4 oxidation reaction of the studied samples [14,17]

Sample	Elemental composition	T_{cal} (°C)	Crystalline phase[a]	S_{BET} (m^2/g)	D_1[b] (nm)	E_a[c] (kcal/mol)	$A_{0\,cor}$[d] (mol/(g s atm))
SS	$LaCo_{0.97}O_3$	1000	P, weak Co	0.4	73.9	25.7	7
COP	$LaCo_{0.98}O_3$	700	P	3.5	32.2	21.0	329
CIT	$LaCo_{0.96}O_3$	600	P	6.6	26.9	20.6	628
RG	$LaCo_{0.80}Fe_{0.20}O_3$	550	P	17.1	16.3	21.7	674
COPRG	$LaCo_{0.93}Fe_{0.03}O_3$	550	P, weak Co	18.7	16.5	20.3	1031
Co1	$La_{0.94}Co_{0.97}Fe_{0.03}O_3$	550	P, weak Co	4.2	16.4	22.4	49
Co2	$La_{0.93}Co_{0.90}Fe_{0.10}O_3$	550	P	10.9	16.4	21.0	498

[a] P, perovskite, Co; cobalt oxide.

[b] Crystal domain size calculated by means of the Scherrer equation $D = \frac{K\lambda}{\beta\cos\theta}$ after Warren's correction for instrumental broadening ($\beta^2 = B^2 - b^2$, where B is the FWHM and b is the instrumental broadening determined by the FWHM of the X-ray reflexion of SiO_2, having particles larger than 150 nm, at $2\theta \approx 27°$).

[c] Activation energy for the methane oxidation reaction, supposing a first-order reaction rate $r = kP_{CH_4}$.

[d] Calculated by linear regression on the Arrhenius plots with E_a fixed at 22.25 kcal/mol, fixed at the mean value of the activation energies E_a obtained by linear regression on the Arrhenius plots.

an amorphous La–Co solid, prepared by coprecipitation, was preferred to the single oxides as a precursor. RG and COPRG were calcined at the same temperature (550 °C). In spite of the different natures of the precursors, the RG and COPRG samples present similar physical properties (Table 1 and Ref. [14]).

Two other ground samples (designated as Co1 and Co2 in Ref. [17] and in this work) were also studied. These two solids were milled under conditions different from those of the RG and COPRG samples (with varying grinding times and different additives). Then, Co1 was ground for only one step, without any additive. This resulted in a low specific surface area (Table 1). Co2 was ground in two steps, like RG and COPRG; however, NaCl was used as an additive instead of ZnO. An intermediate specific surface area (between that of Co1 and those of RG and COPRG) was obtained. As can be observed in Table 1, all of the ground samples present the same crystal domain size (16.3–16.5 nm), but the specific surface areas vary over a large range (between 4.2 m^2/g for Co1 and 18.7 m^2/g for COPRG).

For all of the solids, an important difference between the specific surface area (measured by N_2 adsorption) and the theoretical surface area (calculated from the crystal domain size D_1, supposing a cubic-shaped crystal) is observed. This is explained by the fraction of surface lost by contact between the elementary particles [14], which was previously attributed to the occurrence of grain boundaries between crystals. It was found that the S_{th}/S_{BET} ratio is of great importance in the properties of the solids in TPD-O_2 and in the kinetics of reaction with SO_2 [17].

XRD analysis showed that all of the solids presented the rhombohedral $LaCoO_3$ perovskite structure (JCPDS card 09-0358) (not shown). A weak signal attributed to Co_3O_4 (JCPDS card 42-1467) was also observed for the COPRG, Co1, and SS samples. All of the ground samples present an iron contamination (from $x = 0.03$ for Co1 and COPRG to $x = 0.20$ for RG; Table 1). The degree of iron contamination varies as follows:

$$\text{COPRG} \approx \text{Co1} < \text{Co2} < \text{RG}.$$

2.2. Isotopic exchange experiments (OIE)

To eliminate kinetic limitation due to gas-phase diffusion, the experiments were carried out in a recycling U-shaped microreactor. The recirculation volume was coupled to a quadrupolar mass spectrometer (MQG Blazers). The gas sampling was regulated by a thermo-valve adjusted to maintain a constant pressure of 1×10^{-6} mbar in the ionization chamber. At this pressure, the vacuum sampling leak creates a negligible decrease in the pressure in the microreactor. Twenty milligrams of catalyst was weighed and inserted in a microreactor between two quartz wool plugs. Then the sample was fired at its calcination temperature under O_2 (ramp = 10 K/min $-D_{O_2} = 20$ mL/min). Thereafter, the sample was cooled to room temperature under O_2 and then heated again under dynamic vacuum until the temperature of the test was reached (ramp = 10 K/min). For the exchange experiments, pure $^{18}O_2$ at a pressure of about 70.0 mbar was introduced into the nonheated zone of the recirculation volume (see Appendix A). This allowed us to maintain a constant number of oxygen atoms in the gas phase. This volume of gas was then expended in the heated zone, yielding a pressure of $^{18}O_2$ in the total recirculation volume around 52.0 ± 1.5 mbar, depending on the temperature of the test. In the case of the equilibration reaction, an equimolar volume of $^{18}O_2$ and $^{16}O_2$, instead of pure $^{18}O_2$, was introduced. The partial pressure evolution of $^{18}O_2$ (mass 36), $^{16}O_2$ (mass 32), and $^{16}O^{18}O$ (mass 34) was followed on the mass spectrometer for an experiment time of 90 min. N_2 (mass 28) was also recorded to detect any possible leak. Taking into account the error in the volume of gas introduced into the nonheated zone of the recirculation volume and the error in the temperature, a maximum relative error of 1.0% can be estimated in the values of the initial rates of exchange (Eq. (A.5), Appendix A). For rate values calculated at nonzero times, a third source of error (the decrease in pressure due to the vacuum sampling leak) of 2%/h is added.

2.3. Theory

The exchange mechanism can be described by the following equation:

$$^{18}O_{(g)} + {}^{16}O_{(s)} \Leftrightarrow {}^{16}O_{(g)} + {}^{18}O_{(s)}. \quad (1)$$

Nevertheless, three mechanisms can be distinguished [19, 26–31].

2.3.1. Equilibration reaction

This mechanism results from the adsorption/desorption of an O_2 molecule from the gas phase on the surface of the oxide. This reaction does not require the participation of any oxygen ion from the oxide. Then, the ^{18}O and ^{16}O fractions in the gas phase are constant during the test. This reaction can be written as follows:

$$^{16}O_{2(g)} + {}^{18}O_{2(g)} \Leftrightarrow 2\,{}^{18}O^{16}O_{(g)}. \quad (2)$$

2.3.2. Simple heteroexchange

This exchange occurs with the participation of one oxygen ion from the structure of the solid. The two following equations characterize this mechanism:

$$^{18}O^{18}O_{(g)} + {}^{16}O_{(s)} \Leftrightarrow {}^{18}O^{16}O_{(g)} + {}^{18}O_{(s)}, \quad (3)$$

$$^{18}O^{16}O_{(g)} + {}^{16}O_{(s)} \Leftrightarrow {}^{16}O^{16}O_{(g)} + {}^{18}O_{(s)}. \quad (4)$$

Because of a reaction order to oxygen close to 1 for the oxides presenting this as the main mechanism, Boreskov et al. [32–34] supposed the formation of triatomic species (O_3^-) on the surface (Eley–Riedel mechanism). The formation of a triatomic complex with the two atoms originating from the gas phase and one atom of the surface atomic layer is credible because an oxygen dissociation mechanism on

the surface would present a reaction order to oxygen close to 0.5. According to Winter [28], a dissociative adsorption step requiring an electron transfer from the solid cannot be excluded for certain oxides:

$$O_{2gas} + (e^-|\square s^-: e^-|\square s^-) \Leftrightarrow 2(O^-|\square s^-),$$

with $e^-|\square s^-$, centres F2 Seitz.

O^{2-} from the solid can migrate in the anionic vacancies and associates with O^- for the exchange reaction:

$$\left({}^{18}O^-|\square s^-\right)_1 + \left({}^{16}O^{2-}|\square s^-\right)_2 \Leftrightarrow$$
$$\left({}^{18}O^{2-}|\,\square s^-\right)_1 + \left({}^{16}O^-|\square s^-\right)_2.$$

Desorption occurs when two $(O^-|\square s^-)$, supposedly mobile on the surface, come into contact with each other.

2.3.3. Complex heteroexchange

In contrast to the simple heteroexchange, this mechanism supposes the participation of two atoms of the solid at each step:

$${}^{18}O{}^{18}O_{(g)} + 2{}^{16}O_{(s)} \Leftrightarrow {}^{16}O{}^{16}O_{(g)} + 2{}^{18}O_{(s)}. \quad (5)$$

And in the case of the occurrence of $^{16}O^{18}O$ isotopomers in the gas phase:

$${}^{18}O{}^{16}O_{(g)} + 2{}^{16}O_{(s)} \Leftrightarrow {}^{16}O{}^{16}O_{(g)} + {}^{18}O_{(s)} + {}^{16}O_{(s)}, \quad (6)$$

$${}^{18}O{}^{16}O_{(g)} + 2{}^{18}O_{(s)} \Leftrightarrow {}^{18}O{}^{18}O_{(g)} + {}^{18}O_{(s)} + {}^{16}O_{(s)}. \quad (7)$$

Some oxides were found to present mainly this mechanism of exchange. Then, among the 53 oxides tested in OIE by Winter [28,29], only CuO, AgO, PbO, and Tb_2O_3 were found to present this as the main exchange mechanism. Boreskov et al. [34], who observed an oxygen reaction order near 0.5 for some oxides presenting mainly this mechanism (Cr_2O_3, V_2O_5, α-Fe_2O_3, NiO, etc.), assumed a dissociative adsorption on the anionic vacancies on the surface of the solid. The formation of a quadriatomic intermediate was also considered by some authors [35]. The "place exchange" mechanism, which consists only of the displacement of a preadsorbed O_2 molecule, and which does not require any O–O bond scission, was also proposed as a possible mechanism [36]. The study of superoxide (O_2^-) reactivity, on the surface of $Ce_xZr_{1-x}O_2$, by isotopic exchange followed by FTIR showed that the $^{16}O_2^-$ superoxides exchanged in one step and gave $^{18}O_2^-$ selectively [37]. This corresponds well with a place exchange mechanism.

A mathematical description of the rates of exchange and equilibration, under the conditions of the tests, can be found below (see Appendix A).

3. Results and discussion

3.1. Exchange reaction

3.1.1. Nature of the oxygen exchanged

Fig. 1 presents the different steps to be distinguished during exchange. The first step, (1) in Fig. 1, consists of an adsorption of an O_2 molecule on the surface of the solid. This adsorption is followed by the exchange, with the possible formation of a triatomic surface species [27], or after dissociative adsorption of $^{18}O_2$ in the anionic vacancies, following the mechanism described in [28]. Then, the O_2 exchanged molecule ($^{16}O^{18}O$ in Fig. 1) desorbs. The surface-exchanged ^{18}O atom can then diffuse on the surface (2), in the bulk (3), or in the grain boundaries (4). It is supposed from previous results [14] and other works [15,16,38] that grain boundary diffusion proceeds at a higher rate than bulk diffusion. Then surface and grain boundaries can logically be considered to be quickly exchanged and present the same concentrations of ^{18}O and ^{16}O as the gas phase. Under these considerations, the bulk diffusion proceeds at the same rate, anywhere from the surface or from the grain boundaries (Fig. 1, step $3 + 3'$).

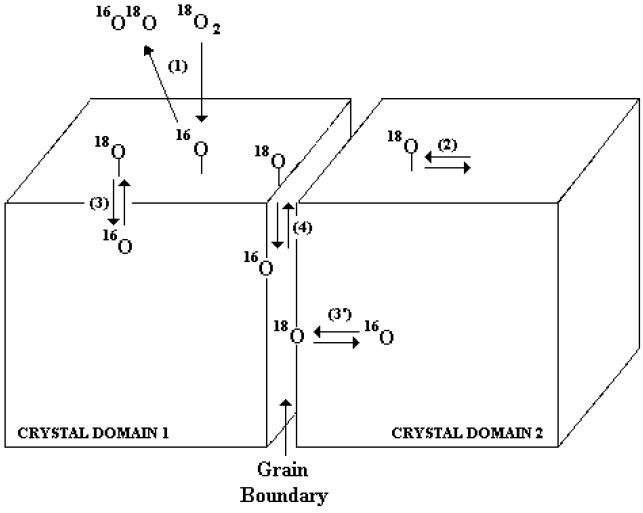

Fig. 1. Scheme of oxygen exchange on $LaCoO_3$.

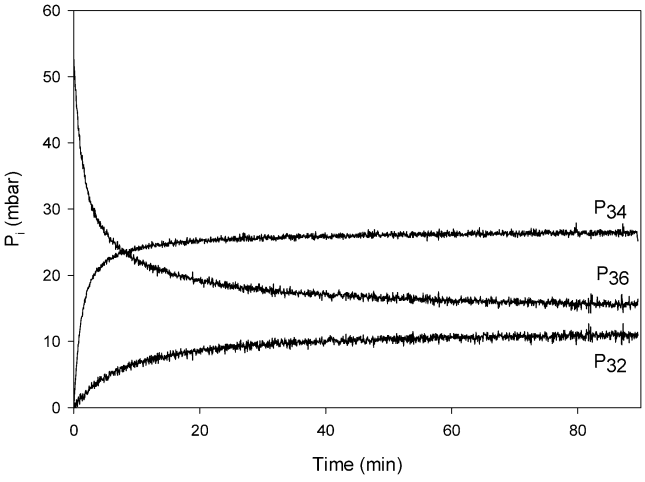

Fig. 2. Evolution of the partial pressure of the different oxygen isotopomers versus time of reaction—CIT exchanged at 539 °C for 90 min.

Results of an exchange experiment, obtained at 539 °C on the CIT sample, are presented in Fig. 2. A decrease in the $^{18}O_2$ partial pressure (P_{36}) with time is observed from the

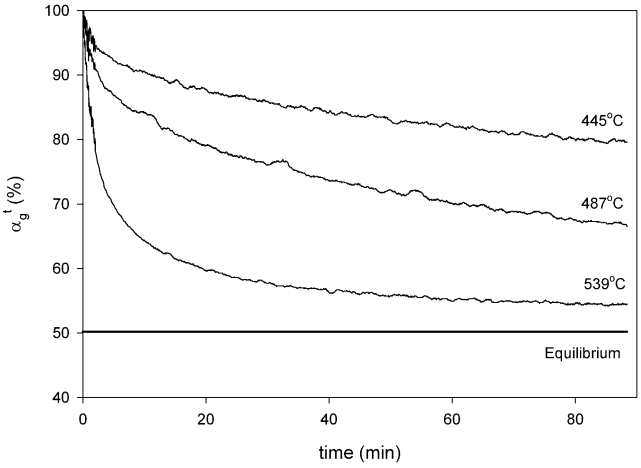

Fig. 3. Evolution of ^{18}O fraction in the gas phase (α_g^t) versus time of reaction—CIT exchanged at different temperatures for 90 min. (Equilibrium is calculated assuming the fractions of ^{18}O in gas phase and bulk solid are equal.)

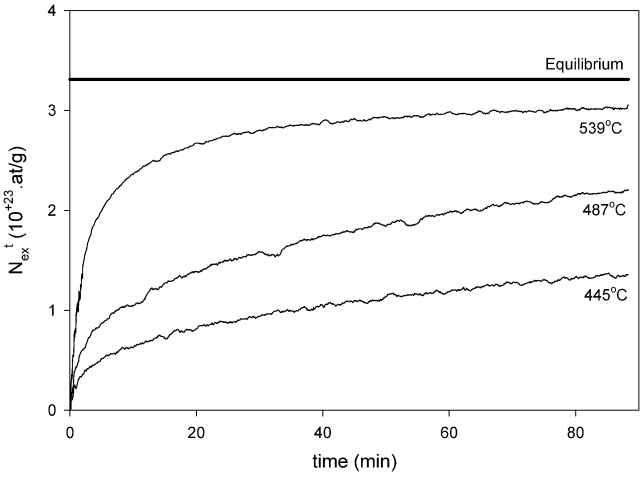

Fig. 4. Evolution of number of atom exchanged (N_{ex}^t) versus time of reaction—CIT exchanged at different temperatures for 90 min. (Equilibrium is calculated assuming the fractions of ^{18}O in gas phase and bulk solid are equal.)

beginning of the test. This decrease is immediately followed by an increase in $^{18}O^{16}O$ partial pressure and, to a lesser extent, by an increase in the partial pressure of $^{16}O_2$ (P_{32}). In the last 30 min, the three partial pressures reached a plateau. The evolution of the ^{18}O fraction in the phase gas (α_g^t) and the number of oxygen atoms exchanged (N_{ex}^t) as a function of time of reaction, obtained for the CIT sample exchanged at different temperatures, are presented in Figs. 3 and 4, respectively. It is clear from these figures that the plateau corresponds to the end of the exchange, when the solid and the gas phase present the same fractions of ^{18}O and ^{16}O. Nakamura et al. [12] already reported a high oxygen mobility in $La_{1-x}Sr_xCoO_3$. The author observed a high activity in exchange for temperatures higher than 300 °C on $LaCoO_3$. An important increase in activity for the exchange reaction with the strontium substitution degree was also reported by the authors. For $La_{0.4}Sr_{0.6}CoO_3$, they observed that, after reaction at 300 °C, all of the oxygen atoms from the solid were exchanged. However, it can logically be supposed that all of the oxygen atoms of $LaCoO_3$ can also exchange at a higher temperature. This is in line with the observation that the exchange proceeds at a higher rate at higher temperatures (Fig. 3), and then the equilibrium is more quickly attained. The results obtained on $LaCoO_3$ strongly differ from the results obtained for $LaFeO_3$ [7] and $LaMnO_3$ [8], which were found to present a low bulk oxygen mobility.

Moreover, the gas phase was verified to be equilibrated. The theoretical gas-phase mole number of $^{16}O_2$ was calculated from those of $^{18}O_2$ and $^{18}O^{16}O$ at each time of the experiment. The calculated partial pressure of $^{16}O_2$ was found in all cases to be equal to the experimental partial pressure (P_{32}), showing the fast equilibration of the isotopomers in the gas phase with the surface (no surface accumulation). The CIT sample, after 90 min of exchange at 539 °C, presents a repartition $P_{34}{:}P_{36}{:}P_{32}$ of 26.5:11.0:15.5 mbar. After complete exchange, the calculated gas-phase partial pressure (from N_g and N_s) would be $P_{34} = 26.6$ mbar, $P_{36} = 13.3$ mbar, $P_{32} = 13.3$ mbar ($P_{34}^2 = 4P_{32}P_{36}$). This is near the values obtained on CIT after 90 min of exchange at 539 °C. It is clear from these results that essentially all of the oxygen of the solid sample is available for exchange (Figs. 3 and 4). Moreover, the exchange limited to the accessible and theoretical surfaces would correspond to a very low decrease in α_g^t (less than 1% for the exchange of the accessible surface and less than 2.5% for the exchange of the theoretical surface). These values are quickly attained in the range of temperature in which the tests were performed, and the time at which they were reached cannot be precisely measured (Fig. 3). In addition, the values of α_g^t attained at the end of the test, largely below the theoretical values calculated for the exchange of the accessible and theoretical surfaces, showed the high mobility of the bulk oxygen.

3.1.2. *Rate of exchange*

The values of the rate of isotopic exchange V_{ex} (Eq. (A.5)) were calculated from the slope of the initial linear part of the exchange curves (Fig. 2). In all cases, the number of atoms exchanged at the end of this linear part largely exceeds the number of atoms exchangeable from the accessible surface (S_{BET}) and from the grain boundaries ($S_{gb} = S_{th} - S_{BET}$). Then the rate of exchange can be considered a measure of the bulk oxygen rate of exchange. The values of V_{ex} obtained at different temperatures are plotted as Arrhenius curves in Fig. 5. The highest activity for exchange is obtained for the COPRG sample. The Co2 and Co1 samples present activities that are similar, but a little lower than that of the COPRG sample. Essentially the same activity was obtained for the RG and CIT samples. Their activities are clearly lower than those of the COPRG, Co2, and Co1 samples. The COP sample presents a lower activity than the ground and CIT samples, and, finally, the lowest activity is obtained for the SS sample. The preexponential factor (A_{ex})

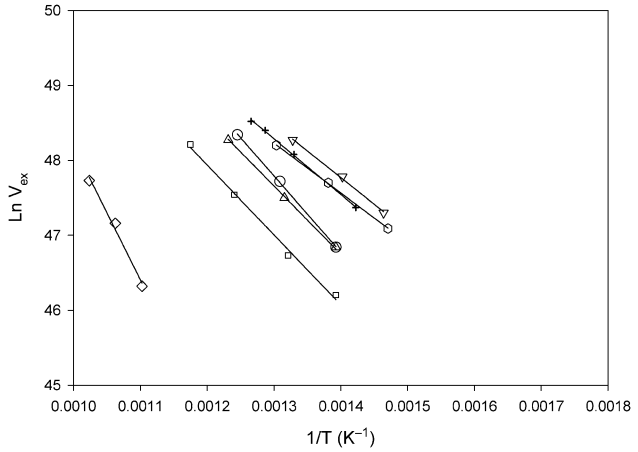

Fig. 5. Arrhenius plots of the initial rates of exchange: +, Co1; ⬡, Co2; ○, RG; ▽, COPRG; △, CIT; □, COP; ◇, SS; Straight line, two parameters (E_{ex} and A_{ex}) linear regression.

Table 2
Isotopic exchange results

Sample	Range of temperature (°C)	E_{ex}[a] (kcal/mol)	A_{ex}[a] (10^{25} at/(g min))	$A_{ex\,cor}$[b] (10^{25} at/(g min))
SS	633–703	35.5	4.9	0.44
COP	445–578	18.6	4.9	3.58
CIT	445–539	17.7	5.1	6.86
RG	445–531	20.1	28.1	7.73
COPRG	373–480	16.1	4.5	17.03
Co1	429–520	14.8	1.5	14.96
Co2	410–496	13.2	0.5	13.40

[a] E_{ex} and A_{ex}, values of activation energy and preexponential factor calculated by linear regression on the Arrhenius plots.

[b] Calculated by linear regression on the Arrhenius plots with E_{ex} fixed at 18.1 kcal/mol.

and activation energy (E_{ex}), obtained by linear regression of the Arrhenius plots (Fig. 5), are summarized in Table 2. The calculated activation energy was found to vary between 13.2 kcal/mol (Co2 sample) and 35.5 kcal/mol (SS sample). Only the SS sample presents an activation energy higher than 20 kcal/mol. This can be explained by the higher temperatures of heating under vacuum for this sample than for the others. As a matter of fact, raising the heating temperature induces the reduction of more Co^{3+} into Co^{2+} on the surface, thus increasing the concentration of the active sites for oxygen exchange. Then the slope of the Arrhenius plot does not correspond to the real activation energy value. Under these considerations, E_{ex} can be considered as constant for all of the tested samples (18.1 kcal/mol, average of the experimental values). To allow a quantitative comparison of the exchange activities, the preexponential factor was recalculated with the common value of activation energy, as in the case of the CH_4 oxidation reaction [14,17]. This regression still yields a reasonable fit for the Arrhenius plots. The corrected preexponential factor ($A_{ex\,cor}$) can be considered a measure of the activity for exchange at all temperatures. The values of $A_{ex\,cor}$ are plotted against the specific surface

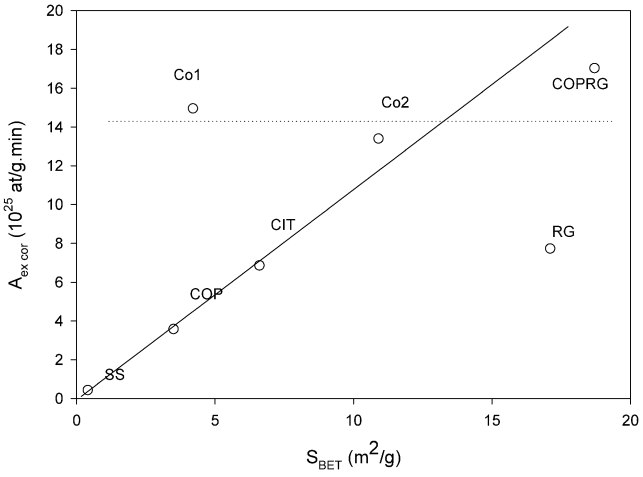

Fig. 6. Corrected pre-exponential factor obtained for the oxygen isotopic exchange as a function of the specific surface area.

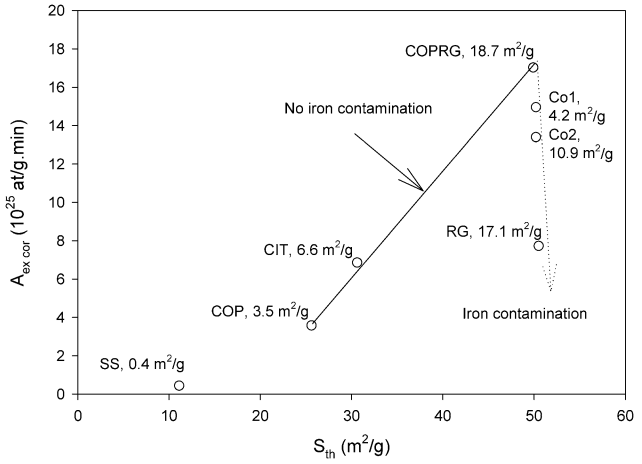

Fig. 7. Corrected pre-exponential factor obtained for the oxygen isotopic exchange as a function the theoretical surface area.

area on Fig. 6. The SS, COP, and CIT catalysts presented an activity that is partially dependent on their specific surface areas (solid line in Fig. 6). However, the ground samples do not satisfy this relation. For example, the CIT sample, which presents a S_{BET} 2.3 times lower than the RG sample, showed a similar activity in exchange. Moreover, the COPRG, Co2, and Co1 presented the highest activities (dotted line in Fig. 6), even though their specific surface areas vary over a large range (from 4.2 m^2/g for Co1 to 18.7 m^2/g for COPRG). In comparison, Co1 (4.2 m^2/g), which presents a specific surface area similar to that of COP (3.5 m^2/g), is clearly more active. A better relation can be obtained between the activity in exchange and the theoretical surface area (Fig. 7). For the same crystal domain size (same theoretical surface area), the same activity is obtained, even if the specific surface area is different (different S_{th}/S_{BET} ratio). Only the SS sample does not satisfy this correlation. Nevertheless, this sample is clearly less active that the others, and its activity for the exchange can be considered to be equal to zero in comparison with those of the other samples (Fig. 7

and Table 2). The differences in activity observed for the different ground samples can be attributed to the iron contamination: the lower the degree of contamination, the higher the activity in exchange (dotted line in Fig. 7). Then the effect of the iron substitution is to decrease the bulk oxygen mobility. This is in line with the observation made by Nitadori et al. [7], who reported a low activity of $LaFeO_3$ in the exchange reaction. Then, it is normal to observe a decrease in oxygen mobility with increasing iron contamination. It was mentioned that surface and grain boundary exchanges were too fast to be measured and only the bulk exchange was measured. Then the rate of exchange is a measure of the bulk oxygen transfer. Under these conditions, it is normal to obtain a rate of exchange depending on the theoretical surface area. Then, the higher the crystal domain size, the lower the theoretical surface area, and then, the lower the rate of exchange.

3.1.3. Mechanism of exchange

We mentioned previously the possible occurrence of two distinct mechanisms of exchange: simple exchange (Eqs. (3) and (4) and complex exchange (Eqs. (5)–(7)). In the case of the $LaCoO_3$ perovskites, the decrease in the gas-phase $^{18}O_2$ concentration followed by the increase in the concentration of $^{18}O^{16}O$, and, to a lesser extent, of $^{16}O_2$, observed in Fig. 1, permit us to conclude that the simple exchange is the main mechanism on these solids (Eqs. (3) and (4)). The simple exchange was observed for a large number of single oxides like SiO_2, Al_2O_3, and ZrO_2 [19,28] and some complex oxides like AFe_2O_4 (with A = Mg, Co, Ni, Zn) [34]. Nevertheless, the complex exchange mechanism (Eqs. (5)–(7)) cannot be excluded. In the case of a pure simple exchange, the initial slope of the P_{32} will be equal to 0, which is not the case here (Fig. 2). The simple exchange can be described in elementary steps:

1. Oxygen adsorption may result from the interaction of a site with an excess of electronic charge (Co^{2+}–□ on Fig. 8) with a gaseous molecule of oxygen.
2. The exchange is the second step. Exchange can proceed with the scission of the O–O bond of the adsorbed molecule [28]. The formation of a triatomic oxygen species $(O_3)^{2-}$ [34] (formed between a surface oxygen (Co^{3+}–O^-) and the adsorbed molecule), as represented in Fig. 8, cannot be excluded. Then, the oxygen molecule exchanges on the surface without scission of the oxygen–oxygen bond. Because of the possible occurrence of some carbonate species on the surface of the samples calcined at low temperature (typically 550–600 °C), it cannot be excluded that some of these surface carbonate species participate in the exchange reaction, as proposed recently by Zhang-Steenwinkel et al. [39], who studied the mechanism of CO oxidation by $^{18}O_2$ on $La_{0.8}Ce_{0.2}MnO_3$.
   Finally, the desorption of the exchanged molecule results in the formation of lattice surface oxygen (Co^{3+}–O^{2-}–$Co^{3+}_{(surf)}$).
3. This lattice oxygen can then decompose to regenerate the initial sites of exchange, or diffuse directly from the surface into the bulk. A parallel mechanism described previously is supposed: quick diffusion in the grain boundaries followed by the diffusion of oxygen from the grain boundaries into the bulk in the same manner as in surface-to-bulk diffusion.

Then the exchange occurs only when a reduced site (Co^{2+}–□) is available for adsorption. This is in line with a Mars–Van-Krevelen mechanism, which is accomplished by alternative reduction and oxidation cycles, and which supposes that the adsorption of an oxygen molecule occurs only when a reduced site is available for adsorption [40].

3.2. Equilibration reaction

The equilibration reaction is described by Eq. (2). The oxygen of the solid does not participate in this reaction. Generally, equilibration proceeds at a lower temperature than exchange. Then, the COPRG, CIT, and RG samples were tested at low temperature in equilibration. The result obtained at 264 °C on COPRG is presented in Fig. 9. The results obtained for the three catalysts are plotted in Arrhenius coordinates in Fig. 10. The preexponential factors (A_{eq}) and activation energies (E_{eq}) obtained by linear regression on the Arrhenius plots are summarized in Table 3. On Fig. 9, a decrease in $^{18}O_2$ and $^{16}O_2$ is observed. These decreases are accompanied by an increase in the $^{18}O^{16}O$ partial pressure. These observations are in line with Eq. (2). However, in all cases, the $^{16}O_2$ partial pressure decrease is slower than that of $^{18}O_2$ and is delayed by about 1 min (Fig. 9). Then, a small decrease in α^t_g is observed. From this result, it is possible to conclude that there is no pure equilibration on this solid at the temperatures of the test, showing that the oxygen desorption step is slow in comparison with the exchange reaction process. In contrast to what was observed by Nakamura et al. [12] on $La_{1-x}Sr_xCoO_3$, who supposed equilibration on their samples, the phenomenon observed in that case is only an exchange with a very slow bulk diffusion and probably slow grain boundary diffusion. This can explain why almost the same activation energy (Table 3) is obtained with the two tests (17.5 and 18.1 kcal/mol for the equilibration and exchange, respectively). Because of the low bulk diffusion coefficient, the measure of the initial rate (V_{eq}) becomes a measure of the surface reactivity. Then, for the three perovskites tested, the same surface reactivity is obtained (Fig. 11). However, it was not possible to know exactly the role of the grain boundary diffusion, which seems to be negligible, from the results presented in Fig. 11.

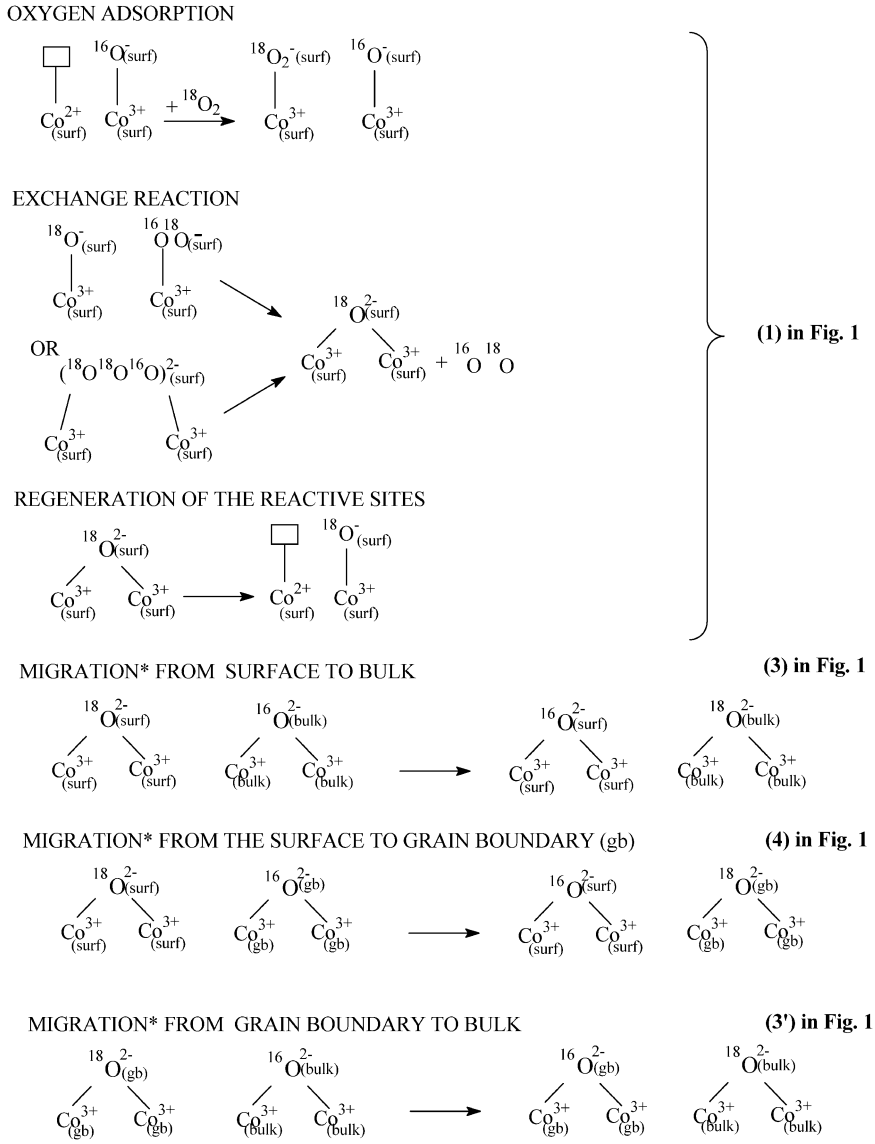

Fig. 8. Elementary steps of exchange on $LaCoO_3$. *, All these mass transfer steps involve also oxygen vacancies.

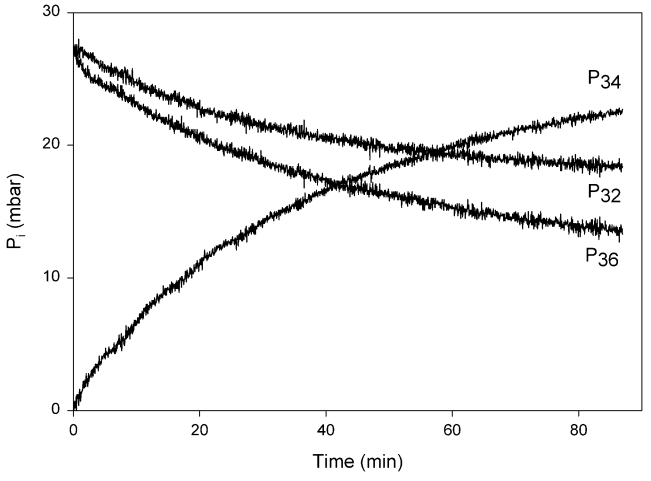

Fig. 9. Evolution of the partial pressure of the different oxygen isotopomers versus time of reaction—COPRG equilibrated at 264 °C for 90 min.

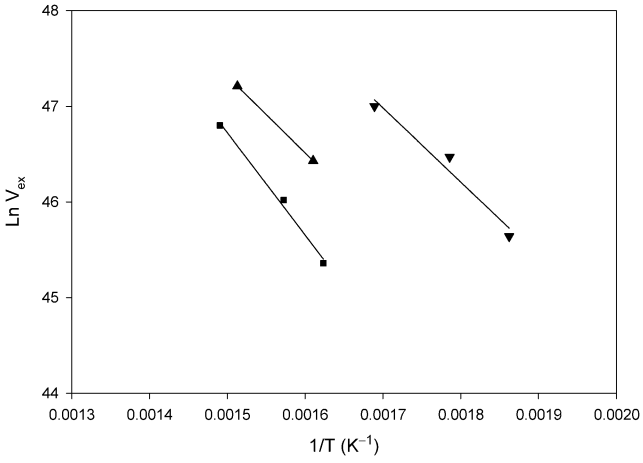

Fig. 10. Arrhenius plots of the initial rates of equilibration: ▼, COPRG; ▲, CIT; ■, COP; Straight line, two parameters (E_{ex} and A_{ex}) linear regression.

Table 3
Isotopic equilibration results

Sample	Range of temperature (°C)	E_{eq}[a] (kcal/mol)	A_{eq}[a] (10^{25} at/(g min))	$A_{eq\,cor}$[b] (10^{25} at/(g min))
COPRG	264–319	15.4	13.5	89.60
CIT	348–388	15.9	5.8	19.71
COP	343–398	21.2	182.4	9.71

[a] E_{ex} and A_{ex}, values of activation energy and preexponential factor calculated by linear regression on the Arrhenius plots.

[b] Calculated by linear regression on the Arrhenius plots with E_{ex} fixed at 17.55 kcal/mol.

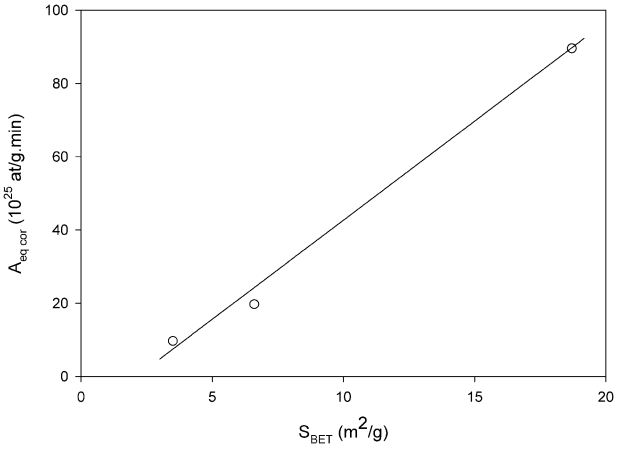

Fig. 11. Corrected pre-exponential factor obtained for the oxygen isotopic equilibration as a function of the specific surface area.

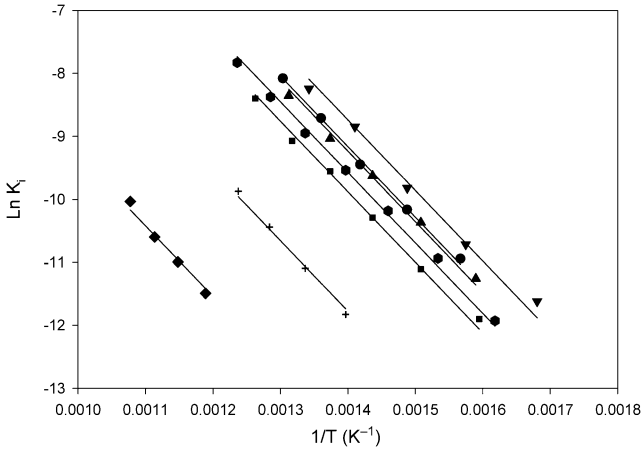

Fig. 12. Arrhenius plots for the first order rate constant k for: +, Co1; ⬢, Co2; ●, RG; ▼, COPRG; ▲, CIT; ■, COP; ◆, SS—Regression lines calculated with $E = 22.25$ kcal/mol [14].

3.3. Role of oxygen in the mechanism of CH_4 oxidation

3.3.1. Activity for methane oxidation

The Arrhenius plots for the first-order rate constant k, obtained for the different samples, are presented in Fig. 12. The values of calculated activation energy (E_a) vary between 20 and 26 kcal/mol (Table 1). As in the case of the OIE reaction, we recalculated the preexponential factor, obtained by direct regression of the Arrhenius plots, by setting E_a to a common value of 22.25 kcal/mol. This still yieds an acceptable fit (solid line in Fig. 12). Then, $A_{0\,cor}$ can be regarded as a quantitative measure of the catalytic activity. Fig. 13 shows the variation of these $A_{0\,cor}$ with the specific surface area. The COP and CIT samples present the same specific activity (line with the higher slope). The same observation is also made for the SS, Co2, and RG samples; however, the lower slope indicates a lower specific activity. The COPRG sample presents a specific activity between those of the two groups, whereas Co1 presents a very low specific activity in comparison with all of the other catalysts. A more detailed analysis of the catalytic activity of these samples for the methane oxidation reaction can be found in Refs. [14,17].

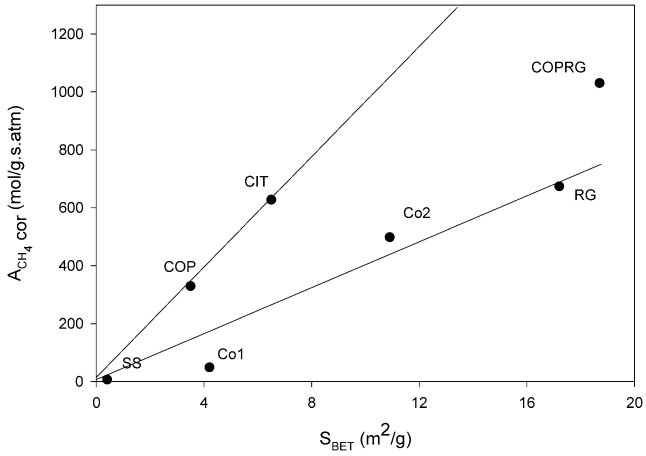

Fig. 13. Corrected pre-exponential factor obtained for the CH_4 oxidation reaction as a function of the specific surface area.

3.3.2. Comparison between the two reactions

Figs. 12 and 13 obtained for the CH_4 oxidation reaction can be compared with Figs. 5 and 6, obtained for the OIE. First, it is observed that the two processes present similar activation energies (18.1 kcal/mol for the OIE and 22.2 kcal/mol for the CH_4 oxidation reaction). A comparison between the normalized activities for the OIE and the CH_4 oxidation reaction is presented in Fig. 14. A clear correlation between the two reactions is obtained for the SS, COP, CIT, RG, and COPRG samples. However, Co1 and Co2 do not satisfy this relation. Indeed, it is observed that the activity for the OIE is similar for the COPRG, Co1, and Co2, whereas large differences, due to the large differences in specific surface areas (Fig. 13), are observed in the CH_4 oxidation reaction. The CH_4 preexponential factors can be plotted as a function of S_{th} (Fig. 15), as in the case of the OIE (Fig. 7). The linear relation observed in the case of the OIE between the COPRG, CIT, and COP is maintained. The SS sample presents an activity that can be considered equal to zero, in comparison with those obtained for the other samples. Then, for these solids, a clear contribution of the bulk oxygen mobility to the rate of the CH_4 oxidation reaction is noticed. From the order of activity obtained for the ground

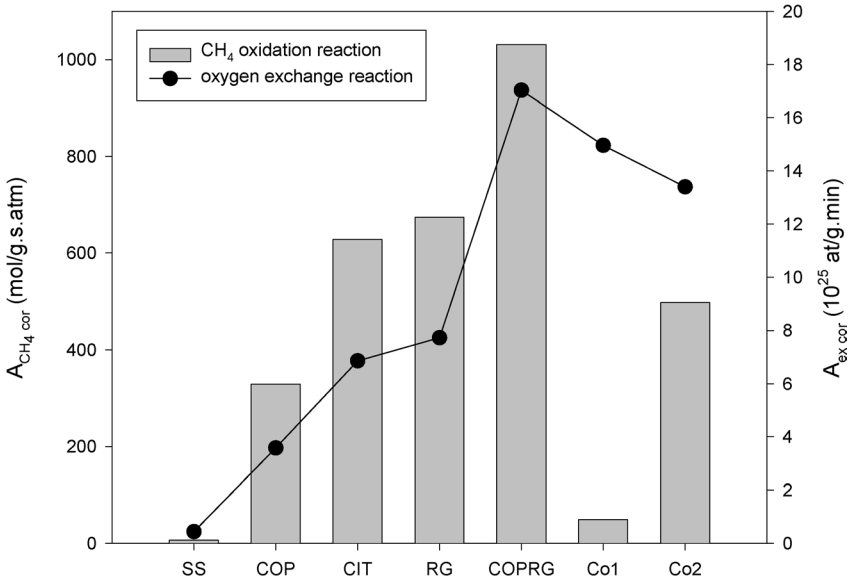

Fig. 14. Comparison of the activities obtained for the methane oxidation reaction and the initial rate of exchange.

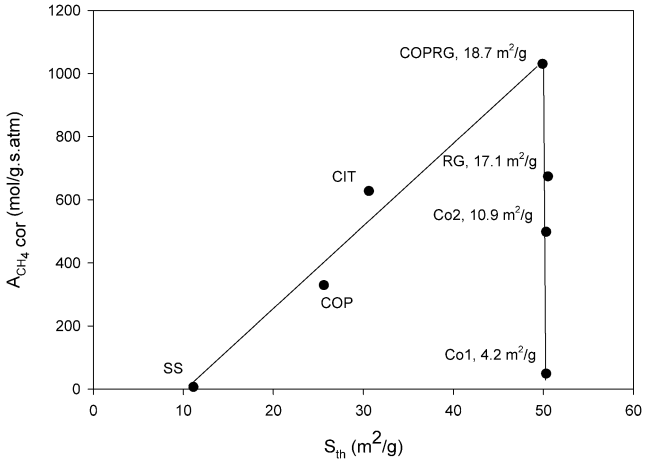

Fig. 15. Corrected preexponential factor obtained for the CH_4 oxidation reaction as a function of the theoretical surface area.

samples, COPRG > RG > Co2 > Co1, we can conclude that, as in the case of the OIE reaction, the crystal domain size and the iron contamination strongly affect the catalytic activity. However, an effect of the accessible surface area is observed for the methane oxidation reaction, which was not observed for the OIE reaction.

According to the Mars–Van-Krevelen mechanism, two independent steps have to be distinguished for the CH_4 oxidation reaction:

$$R + O^* \rightarrow P + {}^*,$$

$$2^* + O_2 \rightarrow 2O^*,$$

where R and P are the reactants and products, O^* is the oxidized sites, and * is the reduced sites. This model assumes that the supply of the oxygen from the gas phase is irreversible and occurs only when a reduced site is available [40]. Then the formation of the oxidation site becomes the limiting factor in the kinetics. In the first part of this work, we supposed a mechanism of exchange (Fig. 8) that implies the adsorption of $O_{2(g)}$ on a reduced cobalt site. Because of the similarity between the OIE and CH_4 oxidation reactions, the same rate-determining step is supposed for the two reactions, and it is the rate of lattice oxygen diffusion, which determines the amount of available active oxygen for the oxidation reaction. However, in contrast to what was observed for the exchange reaction, the effect of the specific surface area noticed in the CH_4 oxidation reaction led us to suppose that not all of the lattice oxygen is available for the reaction. The effect of the specific surface area has been observed by several authors [41–43]. The large differences in activity between two solids of the same composition, but prepared by different methods, were rarely explained only by the specific surface area. For example, Leanza et al. [41] reported an activity for the CH_4 oxidation reaction on $La_{0.9}Ce_{0.1}CoO_3$ prepared by flame-hydrolysis that is one order of magnitude higher than the same solid synthesized by conventional methods. Bell et al. [43] reported a similar observation after testing six $La_{0.7}Sr_{0.3}MnO_3$ synthesized by different routes. The results obtained in OIE for these samples clearly showed the effect of the morphology on the oxygen mobility. It is also shown that the oxygen mobility strongly affects the catalytic activity. Nevertheless, the results obtained for the CH_4 oxidation reaction led us to suppose that only a part of the catalyst is active. A simple model for the description of perovskite morphology is the formation of agglomerates (Fig. 16). Then oxygen mobility is not affected by this agglomeration and depends only on the crystal domain size. The smaller the crystal size, the higher the oxygen mobility. However, the methane access is limited to the external surface area (or BET surface area). Under these considerations, only the outer zone of the agglomerates (Fig. 16) is supposed to be active for the oxidation reac-

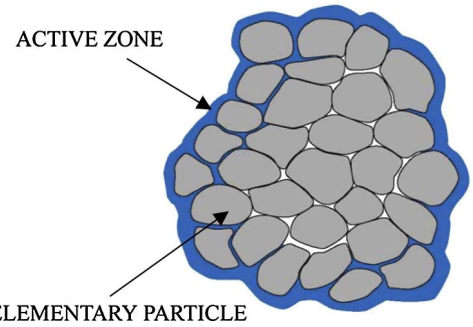

Fig. 16. Schematic view of the active zone for the CH_4 oxidation reaction in an agglomerate formed by several elementary crystals.

tion. Nevertheless, the reactivity strongly differs between the samples (Fig. 13), because of the effect of the crystal size on the oxygen mobility. In this mechanism, the active oxygen availability on the surface is the rate-determining step, and the differences in specific methane oxidation activity are only related to differences in oxygen mobility, generated by the morphological differences.

4. Conclusions

The OIE experiments showed the high reactivity of the oxygen of the $LaCoO_3$ perovskites. It was observed for the tested samples that all of the structural oxygen is available for the exchange. However, large differences in activity were observed between the samples. The activity in OIE was found to correlate well with the theoretical surface, more than with the BET surface area. Then, the samples, which have a lower crystallite size, exhibit the highest activity in OIE. All of the samples present similar activation energies (about 18 kcal/mol). A mechanism that supposes the adsorption of the oxygen from the gas phase on a reduced cobalt site is proposed. Different steps were distinguished: adsorption followed by the exchange reaction and the desorption of the exchanged molecule; formation of lattice oxygen, which can diffuse in the bulk of the solid; and regeneration of the exchange site. It is clear from these results that external accessibility is not a relevant parameter for the exchange, and that oxygen availability is facilitated by quick diffusion along the gain boundaries. In conclusion, OIE seems to be an adequate method for measuring bulk oxygen mobility on cobalt-based perovskites, more so than temperature-programmed oxygen desorption.

These results were compared with results obtained for the methane oxidation reaction. The two processes present similar activation energies (22 kcal/mol for the CH_4 oxidation reaction). In contrast to the OIE reaction, an effect of the BET surface area on the CH_4 oxidation reaction is observed, but the mobility of the bulk oxygen remains of great importance. Then it was possible, with the results obtained for OIE, to explain the differences observed in specific activity in the methane oxidation reaction. The mechanism of oxidation is discussed on the basis of the results obtained for the exchange reaction.

Acknowledgment

Nanox Inc. is acknowledged for the synthesis of samples by reactive grinding.

Appendix A

A.1. Rate of exchange

According to Martin et Duprez [19], the rate of exchange (V_{ex}, at/(g min)) is calculated from the rate of disappearance of ^{18}O from the phase gas at time t:

$$V_{ex} = -2N_g \frac{d\alpha_g^t}{dt} = 2N_s \frac{d\alpha_s^t}{dt}, \tag{A.1}$$

where N_g and N_s are the total number of oxygen atoms in the gas phase and the number of oxygen atoms exchangeable at the surface of the solid;

α_g^t and α_s^t are the ^{18}O atomic fraction in the gas phase and the ^{18}O atomic fraction at the surface at each time.

α_g^t is calculated from the partial pressure of $^{18}O_2$, $^{16}O_2$ and $^{16}O^{18}O$ at each time:

$$\alpha_g^t = \frac{1/2P_{34}^t + P_{36}^t}{P_{32}^t + P_{34}^t + P_{36}^t} \tag{A.2}$$

and N_g is obtained as follows:

$$N_g = \frac{N_A P_T}{R}\left(\frac{V_r}{T_r} + \frac{V_c}{T_c}\right), \tag{A.3}$$

where N_A is Avogadro's number;

P_T is total pressure;

R is the gas constant;

V_r and V_c, are the volumes of the heated and nonheated parts of the system and T_r and T_c are the temperatures of the heated and nonheated parts of the system.

Then the number of exchanged atoms at each time is calculated from the number of ^{18}O atoms at time t:

$$N_e^t = \left(\alpha_g^0 - \alpha_g^t\right)N_g. \tag{A.4}$$

In the test conditions, the initial rate of exchange was calculated from the initial slopes with respect to time of the partial pressure of $^{18}O_2$ ($\frac{dP_{36}^0}{dt}$) and $^{16}O^{18}O$ ($\frac{dP_{34}^0}{dt}$):

$$V_{ex} = -\frac{N_A}{R}\left(\frac{V_r}{T_r} + \frac{V_c}{T_c}\right)\left(2\frac{dP_{36}^0}{dt} + \frac{dP_{34}^0}{dt}\right). \tag{A.5}$$

A.2. Rate of equilibration

The rate of equilibration, described by Eq. (2), is measured by the rate of $^{16}O^{18}O$ formation. Then it can be measured experimentally by

$$V_{eq} = -\frac{N_A}{R}\left(\frac{V_r}{T_r} + \frac{V_c}{T_c}\right)\frac{dP^0_{34}}{dt}. \quad \text{(A.6)}$$

References

[1] W.F. Libby, Science 171 (1971) 499.
[2] R.J.H. Voorhoeve, J.P. Remeika Jr., P.E. Freeland, B.T. Mathias, Science 177 (1972) 353.
[3] H. Arai, T. Yamada, K. Eguchi, T. Seiyama, Appl. Catal. 26 (1986) 265.
[4] T. Seiyama, in: L.G. Tejuca, J.L.G. Fierro (Eds.), Properties and Applications of Perovskite-Type Oxides, Dekker, New York, 1993, p. 215.
[5] G. Kremenic, J.M.L. Nieto, J.M.D. Tascon, L.G. Tejuca, J. Chem. Soc. Faraday Trans. 1 81 (1985) 939.
[6] T. Nitadori, T. Ichiki, M. Misono, Bull. Chem. Soc. Jpn. 61 (1988) 621.
[7] T. Nitadori, M. Misono, J. Catal. 93 (1985) 459.
[8] T. Nitadori, S. Kurihara, M. Misono, J. Catal. 98 (1986) 221.
[9] L. Forni, C. Oliva, F.P. Vatti, M.A. Kandala, A.M. Ezerets, A.V. Vishniakov, Appl. Catal. B 7 (1996) 269.
[10] D. Ferri, L. Forni, Appl. Catal. B 16 (1998) 119.
[11] Y. Ng Lee, R.M. Lago, J.L.G. Fierro, V. Cortés, F. Sapina, E. Martinez, Appl. Catal. A 207 (2001) 17.
[12] T. Nakamura, M. Misono, Y. Yoneda, Bull. Chem. Soc. Jpn. 55 (1982) 394.
[13] R.J.H. Voorhoeve, in: J.J. Burton, R.L. Garden (Eds.), Advances Materials in Catalysis, Academic Press, New York, 1977, p. 129.
[14] S. Royer, F. Berubé, H. Alamdari, R. Davidson, S. McIntyre, S. Kaliaguine, Appl. Catal. A 282 (2004) 273.
[15] N. Sakai, T. Horita, H. Yokokawa, M. Dokiya, T. Kawada, Solid State Ionics 86–88 (1996) 1273.
[16] N. Sakai, http://unit.aist.go.jp/energyelec/fuelcell/english/material/gb-e.html.
[17] S. Royer, A. Van Neste, R. Davidson, S. McIntyre, S. Kaliaguine, Ind. Eng. Chem. Res. 43 (2004) 5670.
[18] H. Abderrahim, D. Duprez, in: A. Crucq, A. Frennet (Eds.), Catalysis and Automotive Pollution Control, in: Stud. Surf. Sci. Catal., vol. 30, Elsevier, Amsterdam, 1987, p. 359.
[19] D. Martin, D. Duprez, J. Phys. Chem. 100 (1996) 9429.
[20] A. Holmgren, B. Andersson, J. Catal. 178 (1998) 14.
[21] A. Holmgren, D. Duprez, B. Andersson, J. Catal. 182 (1999) 441.
[22] C. Descorme, D. Duprez, Appl. Catal. A 202 (2002) 231.
[23] H.X. Dai, C.T. Au, Y. Chan, K.C. Hui, Y.L. Leung, Appl. Catal. A 213 (2001) 91.
[24] S. Szabo, Ph.D. Thesis, Laval University, Québec, 2002.
[25] S. Kaliaguine, A. Van Neste, V. Szabo, J.E. Gallot, M. Bassir, R. Muzychuk, Appl. Catal. A 209 (2001) 345.
[26] E.S.R. Winter, Adv. Catal. Related Subject 10 (1958) 196.
[27] G.K. Boreskov, Adv. Catal. Related Subject 15 (1964) 285.
[28] E.S.R. Winter, J. Chem. Soc. A (1968) 2889.
[29] E.S.R. Winter, J. Chem. Soc. A (1969) 1832.
[30] K. Klier, J. Novakova, P. Jiru, J. Catal. 2 (1963) 479.
[31] J. Novakova, Catal. Rev. 4 (1970) 77.
[32] V.I. Gorgoraki, G.K. Boreskov, L.A. Kasatkina, D. Sokolovskii, Kinet. Catal. 5 (1964) 100.
[33] V.I. Gorgoraki, G.K. Boreskov, L.A. Kasatkina, Kinet. Catal. 7 (1966) 239.
[34] G.K. Boreskov, V.S. Muzykantov, Ann. N.Y. Acad. Sci. 213 (1973) 137.
[35] M. Che, J. Tench, Adv. Catal. 32 (1982) 1.
[36] J. Cunningham, E.L. Goold, J.L.G. Fierro, J. Chem. Soc. Faraday Trans. 78 (1982) 785.
[37] C. Descorme, Y. Madier, D. Duprez, J. Catal. 196 (2000) 167.
[38] A.V. Berenov, J.L. MacManus-Driscoll, J.A. Kilner, Solid State Ionics 122 (1999) 41.
[39] Y. Zhang-Steenwinkel, L.M. van der Zande, H.L. Castricum, A. Bliek, Appl. Catal. B 54 (2004) 93.
[40] M. Stojanovic, C.A. Mims, H. Moudallal, Y.L. Yang, A.J. Jacobson, J. Catal. 166 (1997) 324.
[41] R. Leanza, I. Rossetti, L. Fabbrini, C. Oliva, L. Forni, Appl. Catal. B 28 (2000) 55.
[42] N. Gunasekaran, S. Saddawi, J.J. Carberry, J. Catal. 159 (1996) 107.
[43] R.J. Bell, G.J. Millar, J. Drennan, Solid State Ionics 131 (2000) 211.